An analysis of PEM water electrolysis cells operating at elevated current densities

A. Villagra, P. Millet

An Analysis of PEM Water Electrolysis Cells Operating at Elevated Current Densities

A. Villagra, P. Millet *

Paris-Sud University, ICMMO, Bât. 410, 15 rue G. Clémenceau, 91405 Orsay, France

* corresponding author : pierre.millet@u-psud.fr

ABSTRACT

Recent developments related to the operation of PEM water electrolysis at elevated current density are reported. First, a cost analysis has been performed to discuss the interest of extending the range of operating current density of these cells, towards the 10 A.cm^{-2} range and above. Then the technical impact this may have on the cell design has been analyzed, and the practical conditions required to remove the extra-heat and to facilitate fluid transport across the porous transport layers have been identified. Experimental current-voltage polarization curves have been measured using a pressurized laboratory cells equipped with PFSA (perfluoro-sulfonic acid) membranes of various thicknesses, operating at 80°C and current densities up to 10 A.cm^{-2}. These experimental polarization curves have been fitted using model equations. Key cell parameters such as internal cell resistance, charge transfer exchange current densities and roughness factors have been determined from these fits. The impact of the cell design on the performance and efficiency of PEM water electrolysis cells operated in the multi A.cm^{-2} range of current density has been analyzed, with a focus on the situation that prevails above 5 A.cm^{-2}.

Keywords

Water electrolysis; polymer electrolyte; hydrogen; oxygen; large current density.

1. Introduction

A review of the scientific literature on energy matters over the past decades clearly shows that, due to severe environmental constraints, most (if not all) the energy required for humankind activities should be provided in the (near) future by incident sun light radiations instead of the air-combustion of fossil hydrocarbons or nuclear reactions [1,2]. There is a general agreement among the scientific community that this would avoid the deleterious impact of greenhouse gas emissions on the environment, but would also bring some additional benefits such as the promotion of the energy independency of nations, a reduction of the competition for accessing oil resources, and could also contribute to solve the problems associated with the treatment and long-term storage of nuclear wastes [3]. Such concerns have reached the spheres of policy makers [4] and despite the fact that the so-called *energy transition* is still in its childhood years [5], the concept has received the commitment of most industrialized and developing nations and should, in principle, be on its way. The situation is also attracting new generations of young scientists towards scientific carriers which is an additional good news. The equation that needs to be solved to implement such energy transition on the large scale and turn sun light into renewable electricity is to find an easy and cost affordable manner to transport it over long-distances via power grid infrastructures and to store it. In other words, the *energy transition* will rely on the development of technical solutions for energy storage at different time and size scales. From a practical viewpoint, there is a need to develop an efficient energy infrastructure, adapted to the space and time intermittent nature of earth-incident sun light radiations, and meeting consumers' needs. For technical and cost reasons, electrochemical (batteries) and gravitational storage (*e.g.* via pumped hydro-resources) cannot satisfy these needs. A universal chemical energy carrier that could be used for storage, transportation and distribution of renewable energy, but also for re-electrification by electrochemical or chemical combustion in air, and that could be used as a fuel in the domestic, energy and transport sectors, is required. Gaseous hydrogen of electrolytic grade has been considered for many decades as such a game-changing energy carrier. This

is a by-product of brine electrolysis but it can also be obtained in an efficient and cost affordable way by water electrolysis [6] while the Earth's atmosphere can be used as an oxygen reservoir of infinite capacity (nitrogen dilution is the main drawback of this environment-friendly cycle). Commercial water electrolysers (mostly alkaline technology) are found in quite various fields of the industry but up to now, the technique has been mainly used for stationary production in view of chemical applications. Regarding energy applications (renewable energy production is already a large market, fuel cell mobility is a growing market but large scale energy storage still remains a long-term concept), existing plants of limited size are available only at the demonstration scale [7]. Significant R&D efforts and investments will be necessary before such a *hydrogen economy* [8] becomes reality. The main problem of the *energy transition* is not the concept itself but the time it will take for a large scale implementation. Future water electrolysers will have to be customized to allow non-stationary modes of operation. PEM water electrolysers are commercially available at the multi-MW scale and have already demonstrated their ability to operate under transient power loads [9]. This is why efforts are currently made to develop hundred-MW scale systems.

In this paper, the discussion is restricted to PEM water electrolysis technology. The nominal operating current density (j) is the key parameter that dictates the cost of electrolytic hydrogen and the design and efficiency of the water electrolysis cells. In PEM fuel cells (a sister technology used for the electrochemical combustion of hydrogen in oxygen and the production of electric power), mass transport limitations tend to set the maximum operating current density value in the 1-2 $A.cm^{-2}$ range. Such limitations are not found in PEM water electrolysis cells. Most commercial PEM water electrolysis systems available today on the market operate in the 1-3 $A.cm^{-2}$ range, but there is a trend to extend this range up to much higher values, close to 10 $A.cm^{-2}$ for the oldest reports [10-12], and up to 20 $A.cm^{-2}$ in the most recent ones. This can be achieved by using thin (30-50 micrometer thick) membranes [13,14]. The purpose of this research paper is to report on recent developments in this field and to discuss the impact that such unusually high operating current densities could have on

future system developments. First, a cost analysis is provided to demonstrate the interest of extending the range of operating current density. Then, heat management issues resulting from internal dissipation are analyzed. Mass balance equations are used to determine the optimum water flow required to facilitate heat removal and maintain the temperature increase within limits compatible with membrane stability. The impact of the operating pressure is also analyzed. The volumetric gas and liquid fractions are calculated, with a special focus on the anodic side where counter flows of gaseous oxygen and liquid water are circulating through the pores of these structures. Some experimental limitations such as screening effects observed at the interface between the porous current collector and the membrane-electrode assembly are reported to highlight the problem.

These results have been used to design a cell capable of operation in such conditions and to determine the most appropriate operating parameters for operation at elevated current density. Experimental results measured on laboratory cells operating at 80°C and moderate pressure are reported. Experimental current-voltage polarization curves (I-V curves) have been measured up to 10 $A.cm^{-2}$, using PFSA membranes of various thicknesses. These experimental I-V curves have been fitted using model equations and key cell parameters such as internal cell resistance, charge transfer exchange current densities and roughness factors have been obtained from these fits. The impact of such cell characteristics on the performance and efficiency when the PEM cell is operated in the multi $A.cm^{-2}$ range of current density is discussed, with a focus on the situation that prevails over the 5-10 $A.cm^{-2}$ range. Some perspectives and recommendations are also provided.

2. Optimum operating current density of PEM water electrolysis cells

2.1. The state-of-art and its limitations

The cross-section of a conventional PEM water electrolysis cell is pictured in Figure 1 [15]. The main interests of such “zero-gap” cell is its small thickness (5-7 mm thick on average), its

compactness (that makes dissipation less pronounced than in conventional gap-cells and favor operation at current densities of 1-3 $A.cm^{-2}$), and its lifetime (15,000 to 20,000 hours of operation are common good practice). Such characteristics explain why the technology has been used so far for oxygen generation in places (underwater and space) where compactness prevails over cost and efficiency. The unit cell is delimited by two titanium end-plates (5,5'). The central membrane-electrode assembly (or MEA) (1,2,2') is the heart of the cell. This is the place where liquid water molecules transferred from the anodic chamber (4') are split into gaseous oxygen (2') and hydrogen (2). The interpolar distance between anode and cathode is filled by a thin (50-200 μm thick) proton-conducting perfluorosulfonic acid (PFSA) polymer membrane. The two catalytic layers (20 2') contain a mixture of catalyst particles (in electrical contact) embedded in a PFSA matrix. This is a concept of so-called "3-D electrode" used by electrochemical engineers to increase the overall roughness of catalyst/electrolyte interfaces in order to reduce overvoltages by increasing the value of apparent exchange current densities. Platinum is the most efficient and most stable metal for the hydrogen evolution reaction (HER) in acidic aqueous media. Following trends in fuel cell technology, carbon supported platinum nanoparticles are now used at the cathode (2) of PEM water electrolysis cells instead of unsupported platinum particles, in order to reduce platinum loadings and make the technology cost affordable. Despite a limited bulk electronic conductivity, unsupported iridium dioxide particles are used at the anode (2') to promote the oxygen evolution reaction (OER). Liquid water is pumped across the cells (sometimes through the anode chamber only and sometimes through both anode and cathode chambers) to feed the reaction and for cell cooling purposes. Various cell design are used to provide the necessary voids to pump water flow across the cells and let current flowing from left to right: this can be a grooved bipolar plate or a cell spacer such as a titanium grid (Figure 1, 4-4'). Porous current collectors (3,3') are placed between the MEA and the two cell spacers in order to enable water gas transfers. The critical step is found on the anodic side

where a flow of liquid water from the anodic chamber (4') to the reaction sites (2') meets a counter flow of gaseous oxygen from the anodic catalyst layer (2) to the anodic chamber (4').

During electrolysis ($j \neq 0$), Fermi levels of both anode and cathode are adjusted by using an external DC power supply and electrical current flows across the cell. The transfer of charge carriers (electrons) across the two interfaces induces two redox semi-reactions that evolve molecular hydrogen (cathode) and oxygen (anode). Following the laws of non-equilibrium thermodynamics, a fraction of the electrical energy input is irreversibly transformed into heat by internal dissipation. In the scientific literature, the energy efficiency ε_{cell} of the PEM water electrolysis cell is usually defined as the efficiency of the water dissociation reaction at constant temperature (T) and pressure (P). The energy required to bring tap water to such T,P operating conditions and the energy required by any subsequent gas treatment operation are not taken into account. Different definitions of ε_{cell} are found in the literature. The situation has been recently analyzed by the European Commission in an effort to provide harmonized guidelines [16]. A frequent definition of ε_{cell} is given by Eq. (1). This is the dimensionless ratio of the theoretical amount of energy $\mathbf{W_t}$ (J/mol_{H2}) required at T,P to split one mole of water to the practical amount of energy $\mathbf{W_r}$ (J/mol_{H2}) used in the process. Since liquid water is split in a PEM water electrolysis cell, the reference energy consumption is that of liquid water (absolute value of the HHV of hydrogen combustion in oxygen).

$$\varepsilon_{cell} = \frac{energy\ requirement\ of\ the\ cell\ (reversible\ conditions)}{energy\ provided\ to\ the\ cell\ (irreversible\ conditions)} = \frac{W_t\ (J.mol^{-1})}{W_r\ (J.mol^{-1})} \quad (\mathbf{1})$$

The numerator of Eq. (1) is sometimes defined as the necessary electrical work only. The necessary heat flow ($\Delta Q_{rev} = T.\Delta S$ in $J.mol^{-1}$) required for the entropy change (which is transferred from the thermostat to the cell) is not taken into account and hence:

$$W_t = \Delta G_{rev} = n \cdot F \cdot U_{rev} \textit{ (electrical work)} \quad \textbf{(2)}$$

However, many authors take into account the heat flow required for the entropy change, and hence:

$$W_t = \Delta G_{rev} + \Delta Q_{rev} = \Delta H_{rev} \Leftrightarrow W_t = n \cdot F \cdot U_{rev} \textit{ (electrical} \text{ work)} + n \cdot F \cdot (U_{tn} - U_{rev}) \textit{ (reversible Q)}$$

$$W_t = n \cdot F \cdot U_{tn} \text{ (J/mole) } \textit{(total energy)} \quad \textbf{(3)}$$

At the denominator of Eq. (1), there is a general agreement among authors that W_r is the total (real) electrical energy consumption. This is the necessary electrical work required for the cell/stack plus the extra amount of electrical work which is dissipated internally into heat due to irreversible microscopic processes such as electron charge transfer at interfaces and ionic transport:

$$W_r = \Delta G_{rev} + nF\eta_{loss} \quad \textbf{(4)}$$

$$W_r = n \cdot F \cdot U_{rev} \textit{ (reversible electrical work)} + n \cdot F \cdot (U_{cell} - U_{rev}) \textit{ (irreversible Q)}$$

$$W_r = n \cdot F \cdot (U_{cell}) \text{ (J/mole) } \textit{(total energy = total electrical work)} \quad \textbf{(5)}$$

As a result, the most widely used definition of the water electrolysis cell efficiency is:

$$\varepsilon_{cell}(T,P) = \frac{U_{tn}\,(T,P)}{U_{cell}\,(T,P)} \quad (\mathbf{6})$$

There are concerns in the literature that Eq. (6) could be inappropriate [16]. Care should be taken whenever using that equation, because it is valid only for $U_{cell}(T,P) > U_{tn}(T,P)$. This does not mean that an efficiency larger than 100% is obtained when $U_{rev}(T,P) < U_{tn}(T,P) < U_{tn}(T,P)$. Since the OER overvoltage is large in PEM water electrolysis cells, $U_{cell}(T,P) = U_{tn}(T,P)$ is usually reached

within a few tens of mA.cm^{-2}. This is probably why the definition is commonly used despite its lack of accuracy.

2.2. cell voltage versus current density relationship

The cell voltage $U_{cell}(T,P,j)$ of a PEM water electrolysis cell operating at (T,P,j) conditions where T is the temperature (K), P the pressure (Pa) and j the current density (A.cm^{-2}) is basically the sum of four main cell contributions [17]: (i) the thermodynamic voltage (the necessary reversible heat is provided by the thermostat), (ii) the total ohmic drop inside the cell (including electronic and ionic conduction); (iii) the HER charge transfer overvoltage at the cathode; (iv), the OER charge transfer overvoltage at the anode:

$$U_{cell}(T,P) = \frac{\Delta G(T,P)}{2F} + j\sum_{i=1}^{n} r_i + \left|\eta_{H_2}(T,P)\right| + \eta_{O_2}(T,P) \qquad (7)$$

Where :

- $\Delta G(T,P)$ (in J.mol^{-1}) is the Gibbs free energy change associated to the water splitting reaction under (T,P) conditions.
- F ($96485.33\ C.mol^{-1}$) is the Faraday constant.
- r_i (in Ω.cm^2) is the surface resistance of the ith cell component (cf. Figure 1).
- $\eta_{H_2}(T,P)$ (in V) is the absolute value of the HER overvoltage.
- $\eta_{O_2}(T,P)$(in V) is the OER overvoltage.

More explicitly, the OER and HER overvoltages are calculated using the generalized Butler-Volmer equation for multi-step processes [18]. Both are function of the operating current density, the exchange current density j_0 of each half cell reaction, and the roughness factor of each interface:

$$j^a = j_0^a \, r_f^a \left[e^{\frac{\overleftarrow{\alpha^a} F}{R T} \eta_{O_2}(T,P)} - e^{-\frac{\overrightarrow{\alpha^a} F}{R T} \eta_{O_2}(T,P)} \right] \qquad (\mathbf{8-a})$$

$$j^c = j_0^c \, r_f^c \left[e^{\frac{\overleftarrow{\alpha^c} F}{R T} \eta_{H_2}(T,P)} - e^{-\frac{\overrightarrow{\alpha^c} F}{R T} \eta_{H_2}(T,P)} \right] \qquad (\mathbf{8-b})$$

Where :

- j^a and j^c (both in A.cm^{-2}) are the current density at the anode and cathode.
- j_0^a and j_0^c (both in A.cm^{-2}) are the exchange current density at the anode and cathode.
- r_f^a and r_f^c (adim) are the roughness factors at the anode and the cathode.
- $\overleftarrow{\alpha^a}$ and $\overrightarrow{\alpha^a}$ are the direct and reverse transfer coefficients of the anode.
- $\overleftarrow{\alpha^c}$ and $\overrightarrow{\alpha^c}$ are the direct and reverse transfer coefficients of the cathode.
- R (8.314 J.mol^{-1}.K^{-1}) is the ideal gas constant.

In a first approximation, it can be considered that transfer coefficients are constant (*i.e.* that the rate-determining step of each reaction sequence does not change with the overvoltage).

2.2. Cost requirements

A cost analysis has been performed to identify the most appropriate operating current density for a PEM water electrolysis cell. Both cost and technical aspects have been taken into consideration. There are two major cost contributions to the hydrogen cost (expressed in €.kg$_{H2}^{-1}$) by water electrolysis: (i) the capital expenditure (CAPEX) that takes into account the total

investment cost (the electrolysis stack but also all ancillary equipment, including water purification, AC/DC conversion and gas treatment units) and the lifetime of this investment; (ii) the operational expenditure (OPEX) that takes into account the energy cost and maintenance costs. The optimum current density (j) is the j value that minimizes the hydrogen production cost in €.kg_{H2}^{-1}.

The CAPEX contribution to the total hydrogen cost (in €.kg_{H2}^{-1}) is a function of the initial investment cost IC (in €, *i.e.* the specific power cost in €/kW times the power of the production unit in kW for a hydrogen production at nominal j^{nom} current density), the lifetime T (in seconds) of the electrolysis plant, and the operating current density j (in $A.cm^{-2}$), which all dictate the total amount of hydrogen that the production unit can deliver over its lifetime. Assuming that lifetime of operation is not affected by the operating current density, a straightforward mass balance equation yields the expression of the CAPEX contribution to the hydrogen cost (in €.kg_{H2}^{-1}). Since the investment cost is given for a production unit operating at nominal current density, the CAPEX is inversely proportional to j because over the lifetime T(s) of operation, less hydrogen will be produced if $j < j^{nom}$ and more hydrogen will be produced if $j > j^{nom}$:

$$CAPEX\left(€/kg_{H_2}\right) = \left(\frac{2F(C.mol^{-1}).IC\ (€)}{T(s).S(cm^2).M_{H_2}\left(kg_{H_2}.mol^{-1}\right)}\right).\frac{1}{j(A.cm^{-2})} \qquad (\mathbf{9})$$

According to the roadmap of the European Commission (Horizon 2020 program) reported in the multi-annual work program set out for years 2014-2020 [19], the investment cost for a PEM water electrolyser which was close to ≈ 8 M€.t_{H2}^{-1}.day^{-1} in 2014 (this is equivalent to ≈ 4,000 €.kW^{-1}) should be reduced by a factor of 5 by 2023, down to ≈ 1.5 M€.t_{H2}^{-1}.day^{-1} (this is equivalent to ≈ 750 €.kW^{-1}), in order to open the road (from 2023 onwards) to large scale deployment. In 2018, the investment cost was already close to ≈ 3 M M€.t_{H2}^{-1}.day^{-1} (this is equivalent to ≈ 1,500 €.kW^{-1}): a further reduction by a factor two is still needed.

The OPEX contribution to the hydrogen cost in €.kg_{H2}^{-1} is a measure of the hydrogen production cost. This is mainly the sum of energy and maintenance costs (in a first approximation, water consumption and the energy required for water purification can be neglected when tap water that meets European quality standards is available onsite). The OPEX is obviously a function of the operating current density j (and the cell voltage via the I-V curve) and a function of the electricity cost EC (in €.kWh^{-1}). Assuming that the energy consumption of ancillary equipment can be neglected compared to the electricity consumption of the electrolysis stack (90-95%), a mass balance equation yields the expression of the OPEX contribution to the hydrogen in €.kg_{H2}^{-1}:

$$OPEX\left(€.kg_{H_2}^{-1}\right) = \frac{U_{cell}(V).F(C.mol^{-1})}{3600(J.kg.kWh^{-1}.mol^{-1})}\ .EC\ (€.kWh^{-1}) \qquad (\mathbf{10})$$

In Eq. (10), the OPEX is a function of the operating current density j via U_{cell}(V) which is related to j by Eq. (7). Over a lifetime of T seconds, the total hydrogen cost (in €.kg_{H2}^{-1}) is calculated by summing the CAPEX (investment, excluding civil engineering cost) and the OPEX (energy and maintenance costs) contributions. A typical example is provided in Figure 2. Figure 2-a shows the reference I-V curve and the nominal operating current density of 2 A.cm^{-2} used in the calculation. Figure 2-b shows the CAPEX and OPEX cost contributions to the total hydrogen cost as a function of j. Calculations were made using Eqs. (9) and (10), assuming an investment cost of IC = €1,500/kW, an electricity cost of €150/MWh, and a lifetime T of 20,000 h. There is a clear exponential decrease of the CAPEX with operating current density. This is obviously because the size (and hence the cost) of the production unit depends strongly on current density. At low j values, the electrolyser will produce a limited amount of gases during its lifetime, while at high current density significantly more will be produced. Regarding the OPEX dependence on current density, it arises from the current–voltage characteristics of Figure 2-a. The cost increases logarithmically at

low current density and then linearly at higher current densities because of internal power dissipation in the cells. The lower the operating current density, the lower the OPEX: ≈ 100% efficiency can be reached in reversible conditions only, when the cell voltage is close to the thermodynamic voltage, as shown by Eq. (9). Therefore, it can be concluded that CAPEX and OPEX have opposite trends with j. A reduction of the CAPEX requires an increase in operating current density while, simultaneously, a reduction of the OPEX requires a decrease in operating current density. As a result of these two opposite trends, there is an optimal current density value which, of course, depends mainly on the cost of kWh of electricity. On Figure 2-b, the optimum was found to be at ≈ 2.5 $A.cm^{-2}$. The higher the cost of electricity, the narrower and the lower are the range of current density of interest, and vice versa. Conversely, when the electricity cost decreases (a current trend resulting from the deployment of cost-affordable PV panels), the optimum current density value that minimizes the hydrogen cost tends to increase towards the 10 $A.cm^{-2}$ range. Up to the MW-scale, the CAPEX contribution to the total hydrogen cost tends to decrease. Projections show that for electrolysers larger than 1 MW, the CAPEX contribution falls down to ≈ 20% of the total hydrogen cost [20]. For such systems, the energy consumption is the key parameter that drives the hydrogen cost. Significant R&D efforts will be required in the future in material and polymer science to develop enhanced electrocatalysts membranes. A useful criterion that can be used to compare laboratory practices and commercial technologies is the operating current density across the cell at a maximum cell voltage of 2 volt (this threshold value is dictated by the ability of unprotected titanium-based cell components to resist to oxidation): 2-3 $A.cm^{-2}$ at 2 Volt is common good practice but it can be expected that in the near future, the operating current density of interest will be shifted to higher values, closer to 10 $A.cm^{-2}$. Based on these different considerations, it can be concluded that there is an economical interest for operating PEM water electrolysis cells at elevated current densities but the design of the cells has to be adapted to maintain a good efficiency. Main design constraints are analyzed in the following sub-sections.

2.3. Heat management requirements

During electrolysis (j ≠ 0), electrical energy is irreversibly dissipated into heat. Dissipation takes place mainly in the membrane (as a result of proton transport) and in the catalytic layers (as a result of charge transfer processes across both interfaces). The resulting heat must be extracted from the cell in order (i) to maintain the maximum cell temperature value below a threshold value of approximately 80-90°C, a value usually dictated by the thermal stability of PFSA materials used as polymer electrolyte in the cell; (ii) to avoid the formation of thermal gradients that can cause differential PFSA swelling, mechanical stress and performance degradation, especially in the catalyst layers. During electrolysis, liquid water is pumped through the cell/stack to feed the reaction at the anode, but most importantly, to extract the heat produced by internal dissipations and to monitor the cell temperature. For sake of simplification, let us consider a case when liquid water is pumped through the anode compartment only and when all the heat is extracted from the anodic water circuit. This is a reasonable assumption for two main reasons: (i) the OER overvoltage is much larger than the HER overvoltage; (ii) the electro-osmotic water drag that comes across the membrane from anode to cathode and cools down both membrane and cathode is usually recycled to the anode circuit. Let us introduce the λ_{H_2O} factor of Eq. (11) to relate the operating cell voltage U_{cell} to the maximum water ΔT. This is a factor used to characterize the water flow pumped through the PEM water electrolysis cell. This is the dimensionless ratio of the total water flow pumped through the cell/stack to the water flow electrolyzed at the anode of the cell:

$$\lambda_{H_2O} = \frac{2F}{M_{H_2O}\, C^{p}_{H_2O}\, \Delta T}\,(U^{cell} - U^{tn}) \qquad (\mathbf{11})$$

where :

- λ_{H_2O} is the dimensionless and time independent ratio of the actual water flow in circulation to the flow of water which is electrolyzed at the current density j of operation.
- F = 96485.33 C.mol^{-1} is the Faraday constant.
- M_{H_2O} = 18 g.mol^{-1} is the molar weight of water.
- $C_{H_2O}^{p}$= 4.18 J.g$_{H2O}^{-1}$.K^{-1} is the heat capacity of liquid water at constant pressure.
- ΔT in Kelvin is the water temperature difference between cell outlet and inlet.
- U^{cell} in volt if the cell voltage of operation.
- U^{tn} in volt is the thermoneutral cell voltage at the T,P conditions of operation.

Figure 3 shows a plot of λ_{H_2O} versus the cell/stack ΔT for different operating cell/stack voltages. Small ΔT values require very large water flows (and hence λ_{H_2O} >> 1) and vice versa. Water needs for cooling purposes increase with an increasing operating cell voltage. It should be noted here that, since the operating cell voltage tends to increase with time, the heat extraction requirements are not the same at the beginning of life (BoL) and end of life (EoL) of the cell/stack. Optimal λ_{H_2O} values should therefore be calculated for EoL cell voltages, if the pump used in the process operates at constant water flow.

In the temperature range of operation of PEM water electrolysis cell/stack (50-80°C), the thermal conductivity of oxygen is approximately 25 times less than the thermal conductivity of liquid water. Large gas volumetric fractions and gas screening effects in compartments 4 and 4’ (Figure 1) can potentially hamper heat extraction from the cell/stack. It is therefore useful to calculate the mean liquid and gas volumetric fractions inside the cell/stack as a function of operating temperature and pressure to adjust the operating pressure to the operating current density. The volumetric water flow rate pumped through the PEM cell/stack at T,P,j, λ_{H2O} and ΔT operating conditions of interest is given by:

$$\dot{v}_{H_2O}\ (m^3.s^{-1}) = \frac{M_{H_2O}\ j\ S_{EC}^{tot}}{2\ F\ \rho_{H_2O}} \lambda_{H_2O} = \frac{j\ S_{EC}^{tot}\ (U^{cell} - U^{tn})}{C_{H_2O}^{p}\ \rho_{H_2O}\ \Delta T} \qquad (\mathbf{12})$$

In Eq. (12), $S_{EC}^{tot} = N\ S_{EC}^{cell}(cm^2)$ is the total electrochemical surface area in cm^2: this is the product of the cell number N by the individual surface area; $\dot{v}_{H_2O}\ (m^3.s^{-1})$ is calculated using $M_{H_2O} = 18x10^{-3}\ kg.mol^{-1}$, $C_{H_2O}^{p} = 4.187\text{x}10^3\ \text{J.kg}^{-1}.\text{K}^{-1}$ and $\rho_{H_2O} = 10^3\ \text{kg.m}^{-3}$.

The volumetric oxygen flow rate at the same T,P,j, λ_{H2O} and ΔT conditions of interest is given by:

$$\dot{v}_{O_2}\ (m^3.s^{-1}) = \frac{j\ (A.cm^{-2})\ S_{EC}^{tot}(cm^2)}{4\ F}\ \frac{R\ (8.314\ MKSA)\ T\ (K)}{P\ (bar)x10^5} \qquad (\mathbf{13})$$

Combination of Eqs. (12) and (13) yields the volumetric fractions of liquid water and gaseous oxygen:

$$x_{liq}(\%) = x_{H_2O}(\%) = \frac{\dot{v}_{H_2O}(m^3.s^{-1})}{\dot{v}_{H_2O}(m^3.s^{-1}) + \dot{v}_{O_2}(m^3.\text{h}^{-1})} \qquad (\mathbf{14})$$

$$x_{H_2O}(\%) = \frac{\dfrac{(U^{cell} - U^{tn})}{C_{H_2O}^{p}\ (4.187\text{x}10^3\ \text{J.kg}^{-1}.\text{K}^{-1})\rho_{H_2O}\ (10^3\ \text{kg.m}^{-3})\Delta T}}{\dfrac{(U^{cell} - U^{tn})}{C_{H_2O}^{p}\ (4.187\text{x}10^3\ \text{J.kg}^{-1}.\text{K}^{-1})\rho_{H_2O}\ (10^3\ \text{kg.m}^{-3})\Delta T} + \dfrac{R\ (8.314\ MKSA)\ T\ (K)}{4\ F\ P\ (bar)x10^5}} \qquad (\mathbf{15})$$

$$x_{gaz}(\%) = 1 - x_{liq}(\%) = x_{O_2}(\%) = \frac{\dot{v}_{O_2}(m^3.\mathrm{h}^{-1})}{\dot{v}_{H_2O}(m^3.s^{-1}) + \dot{v}_{O_2}(m^3.\mathrm{h}^{-1})} \qquad (\mathbf{16})$$

Figure 4 shows a plot of liquid water and gaseous oxygen volumetric fractions versus operating cell/stack pressure for different cell ΔT. For low ΔT values (ΔT < 5°C), a large amount of liquid water is pumped through the cell/stack and therefore, the volumetric fraction of liquid water is larger than 95% at atmospheric pressure. However, for lower λ_{H_2O} values (ΔT > 5°C), the water flow pumped through the cell/stack is much smaller and the liquid fraction decreases accordingly. These results show that pressurization up to 5 bars is sufficient to maintain the gas fraction to less than 10%. In conclusion, the water volumetric flow pumped through a PEM cell/stack is a trade-off between different factors: (i) the energy required to pump that water flow; (ii) the max ΔT acceptable to reduce ageing rates and degradation processes; (iii) the heat transfer rates that also set the maximum temperature of the cell, which in turn dictates the durability. The volumetric gas fraction can be reduced by increasing the operating pressure, a condition which also favors heat extraction.

2.4. Volumetric fractions of water and oxygen across the anodic PTL

Another problem requiring attention is the mass transport situation that prevails at the anode during operation (j ≠ 0). Porous transport layers (PTL) used on both anode (cell component 3 in Figure 1) and cathode (cell component 3’ in Figure 1) sides are key cell components. A PTL is sometimes called a porous current collector (PCC), when the focus is placed on current conduction through the bulk solid phase instead of mass transport through internal pores. During operation (j ≠ 0), liquid water is transferred through the PTL from the anodic compartment (4’ in Figure 1) to the anodic catalyst layer (2’ in Figure 1): the driving force is the gradient of water chemical potential, which is a combination of pressure and concentration gradients across the PTL. At the same time,

gaseous oxygen is transported backwards, from the anodic catalytic layer (2' in Figure 1) to the anodic compartment (4' in Figure 1): a driving force of similar nature is acting but the gradient is in the opposite direction. At low operating pressures (close to ambient pressure), mass transport limitations are sometimes observed when the porosity of the PTL and/or the tightness of the cell are inappropriate, even at low operating current density, as shown in Figure 5 [21]. This is obviously a limit that needs to be overcome to operate the cell at much higher operating current densities.

Up to now, there is no clear understanding of the mechanism of water/O_2 cross-transport across a PTL. What is well established is that there is no need to use two specific networks of channels, one for the liquid (water) phase and one for the gas (oxygen) phase. Experimentally, there is however no clear evidence showing that the process is either stationary (co-existence of stationary liquid and water flow in opposite directions) or transient (evacuation of bursts of oxygen gas once the oxygen pressure reaches a critical threshold value). The situation and transport mechanisms are expected to be different at low operating current density (transport of isolated oxygen bubbles across pores filled with liquid water) and at elevated current density where most of the volume is occupied by the gas phase (hydrophilic internal pore are supposed to favor annular transport of liquid water along pore walls while empty bulk pore regions are supposed to favor gas transport). In order to put into evidence the intuitive effect of operating pressure on the process, but on a more quantitative basis, it is necessary to calculate both flows. The liquid water and gaseous oxygen flows are simply related to the operating current density. It is therefore easy to calculate the volumetric fraction of each of them across the PTL, as a function of operating pressure. The specific flow of liquid water from the anode compartment (4' in Figure 1) to the anode (2' in Figure 1) required to feed the OER at a current density of j ($\dot{v}^1_{H_2O}$) is given by :

$$\dot{v}^1_{H_2O}(cm^3.s^{-1}.cm^{-2}) = \frac{j}{2F}\frac{M_{H_2O}}{\rho_{H_2O}} \qquad (\mathbf{17})$$

Where, again, j is the operating current density in A.cm^{-2}, F is the faraday, M_{H_2O} is the molar weight of water (18 g.mol^{-1}), and ρ_{H_2O} is the volumetric weight of water (≈ 1 g.cm^{-3} over the T,P range of interest). The specific flow of liquid water from the anode compartment (4' in Figure 1) to the anode (2' in Figure 1) required for the electro-osmotic flow of protons across the membrane ($\dot{v}^2_{H_2O}$) is given by:

$$\dot{v}^2_{H_2O}(cm^3.s^{-1}.cm^{-2}) = \frac{j\,n}{F}\,\frac{M_{H_2O}}{\rho_{H_2O}} \qquad (\mathbf{18})$$

Where n (with unit of $mol_{H2O}/mole_{H+}$) is the stoechiometry factor that gives the number of water molecules required for hydrating one proton. For PFSA materials (such as Nafion®) having an equivalent weight EW = 1100 eq.g^{-1}, this is usually close to 4 but n can vary significantly as a function of a large number of parameters (both operating and linked to the treatment of the membrane). According to Eqs. (17) and (18):

$$\frac{\dot{v}^2_{H_2O}(cm^3.s^{-1}.cm^{-2})}{\dot{v}^1_{H_2O}(cm^3.s^{-1}.cm^{-2})} = 2\,n \qquad (\mathbf{19})$$

The specific counter flow of gaseous oxygen from the anode catalytic layer (2' in Figure 1) to the anode compartment (4' in Figure 1) resulting from water dissociation at the anode is given by:

$$\dot{v}_{O_2}(cm^3.s^{-1}.cm^{-2}) = \frac{j}{4F}\,\frac{10^6 R\,T}{P} \qquad (\mathbf{20})$$

Where R is the ideal gas constant (R = 8.314 J.mol^{-1}.K^{-1}), T is the operating temperature in K and P the operating pressure in Pa. The volumetric fractions of liquid water x_{H_2O} and gaseous oxygen x_{O_2} across the PTL at T,P operating conditions are obtained by combination of Eqs. (17), (18) and (20) and found to be independent of j:

$$\frac{x_{H_2O}(\%)}{100} = \frac{\dot{v}^1_{H_2O} + \dot{v}^2_{H_2O}}{\dot{v}^1_{H_2O} + \dot{v}^2_{H_2O} + \dot{v}_{O_2}} = \frac{\frac{M_{H_2O}}{\rho_{H_2O}}\left(\frac{1}{2}+n\right)}{\frac{M_{H_2O}}{\rho_{H_2O}}\left(\frac{1}{2}+n\right) + \frac{10^6 R\,T}{4\,P}} \qquad (\mathbf{21-a})$$

$$\frac{x_{O_2}(\%)}{100} = \frac{\dot{v}_{O_2}}{\dot{v}^1_{H_2O} + \dot{v}^2_{H_2O} + \dot{v}_{O_2}} = \frac{\frac{10^6 R\,T}{4\,P}}{\frac{M_{H_2O}}{\rho_{H_2O}}\left(\frac{1}{2}+n\right) + \frac{10^6 R\,T}{4\,P}} \qquad (\mathbf{21-b})$$

Figure 6 shows a plot of the water (Eq. 21-a) and oxygen (Eq. 21-b) volumetric fractions inside the PTL as a function of operating pressure. At atmospheric pressure, the volumetric fraction of liquid water inside the pores of the PTL is only 1% and that of gaseous oxygen is 99%. At 50 bars (the maximum operating pressure of most PEM systems), this is 36% and 64%.

3. The PEM Water electrolysis cell operating in the multi A.cm^{-2} range

Based on the conclusions of the previous section, a PEM water electrolysis cell capable to operate up to 10 A.cm^{-2} has been designed and used to measure experimental I-V curves.

3.1. Experimental details

Perfluorosulfonic acid (PFSA) polymer membranes (Nafion® 117, 115, 212 and 211) have been used to prepare the different MEAs. Dry thicknesses are reported in Table1. Platinum on carbon (40 wt.%, 0.5 mg.cm^{-2}, Johnson Matthey, UK) has been used as electrocatalyst at the cathode for the HER. Unsupported iridium dioxide particles (Surepure Chemetals, USA) have been

used as electrocatalyst at the anode for the OER. The catalyst layers (mixtures of catalyst particles and PFSA chains) have been deposited onto the membrane by spraying a solution (50-50 vol.% of water and isopropanol). I-V curves have been measured using a 7 cm^2 laboratory mono-cell designed for operation at elevated current density. The cell was equipped with two thick end plates with machined flow fields to facilitate water circulation with λ_{H2O} values up to 200, in order to remove extra heat produced at elevated current density. The cell contained two titanium porous transport layers (PTL, 50% open porosity, GKN Co.), one at the anode and one at the cathode. A dedicated experimental setup has been used to measure the I-V curves. Thermostated (Bioblock/Huber thermostat) and de-ionized (Milli-Q® grade) water has been pumped through both anode and cathode cell compartments. A 0-10Volt/0-100A DC power supply (Powerbox, Craftec Co.) has been used for operation in galvanostatic conditions. Pressure transducers and regulators (Keller Co.) have been used for pressure measurement and monitoring.

3.2. Experimental results

Polarization curves (*i.e.* plots of current density versus cell voltage or I-V curves) have been measured at constant operating temperature and pressure up to 10 $A.cm^{-2}$ using the 7 cm^2 laboratory PEM water electrolysis cell designed for operation at elevated current density. A typical result obtained with a Nafion® 117 MEA is shown on Figure 7. The I-V curve (black circles, left Y axis) measured at 80°C exhibited two characteristics domains: (i) the activation domain at low ($j < 1.0$ $A.cm^{-2}$) current density where the ohmic drop associated with the internal cell resistance is low and where charge transfer overvoltages predominate; (ii) the ohmic domain where charge transfer overvoltages can be considered as constant and where the voltage drop resulting from the internal cell resistance predominates. The second curve (red circles, right Y axis) is a plot of the first j derivative of the I-V curve as a function of j: this is a plot of the cell resistance in $\Omega.cm^2$. The value of ≈ 250

mΩ.cm^2 obtained for large j values is characteristic of a PEM water electrolysis cell operated at 80°C with a Nafion® 117 membrane. Figure 8 shows five different I-V curves measured at 80°C and 15 bars up to 10 A.cm^{-2}, using PFSA membranes of different thickness (black circles): (a) 178 μm; (b) 178 μm; (c) 127 μm; (d) 51 μm; (e) 25 μm. Water splitting efficiency values are shown by horizontal dotted bleu lines (calculated using Eq. 6).

3.3. Performance analysis

Four different domains are delineated on the I-V plot of Figure 8 by using thick red dotted lines. The first domain (I) is not directly accessible to the operator: this is the domain where cell voltages are less than the minimum thermodynamic requirement. The second domain (II) is the usual domain of operation of PEM water electrolysis cells, with cell voltages up to 2 Volt and current densities up to a maximum of a few A.cm^{-2}. The third domain (III) is the high current density region which is already accessible today using commercially available PFSA and cell materials, but which requires cell voltages well above 2 Volt (a critical value for titanium collectors which are prone to massive oxidation above that threshold) and corresponding low efficiencies. The fourth and last domain (IV) is the most interesting one: it is not accessible yet, and R&D efforts are still needed to make PEM water electrolysis cells operating at such elevated current densities with efficiencies > 75%. In order to identify the most significant cell parameters that dictate the cell performances, the different I-V curves of Figure 8 have been fitted [17] using the model Eq. (7). Best fit have been obtained using an automated least-square procedure [22]. Fit parameters are compiled in Table 1. In Eq. (7) main operating parameters such as temperature and pressure, the various (electronic, contact and ionic) internal cell resistances, anodic (OER) and cathodic (HER) exchange current densities and the roughness factor of the two catalyst layers were taken into account. Exchange current densities used in the fit for the HER and OER were those measured on smooth platinum and iridium dioxide

electrodes respectively [17]. The micro-structure of the two catalytic layers has been taken into account in a simple way by introducing the two roughness factors r_f^a (Eq. 8-a) and r_f^c (Eq. 8-b) which are defined as the dimensionless ratio of the total electrode/electrolyte interface area (in cm^2) to the geometrical surface area (in cm^2). Typical roughness values can go up to a few hundred, depending on the nano-structuration of the electrodes.

For the four experimental I-V curves of Figure 8, best fits were obtained by setting exchange current densities to constant values because in the four cases, the same electrocatalysts were used at the anode (IrO_2) and at the cathode (Pt/C). Internal cell resistances were calculated by taking the ionic resistivity and the thickness of the different membranes used in the experiments and by adding the constant non-ionic resistance of the 7 cm^2 cell. Experimental I-V curves were fitted by setting the cathodic roughness factor to a constant value of 150 (a characteristic value for this type of HE electrocatalyst), and by adjustment of the anodic roughness factor r_f^a only. Best fits were obtained for $5 < r_f^a < 75$, a characteristic of unsupported IrO_2 particles. Above ≈1.7 Volt, overvoltages became almost constant. The main cell voltage contribution that determines the slopes of the I-V curves was the membrane resistance. Domain (IV) of the plot with $j > 5$ $A.cm^{-2}$ is the target domain. It will become accessible in the future when sufficiently thin (but still mechanically resistant and also resistant to gas cross-permeation [23]) PFSA membranes will become available. A hypothetical case (curve e) obtained with similar catalysts but using a 25 μm thick membrane has been plotted in Figure 8 for comparison: almost 7 $A.cm^{-2}$ were passed for a maximum cell voltage of 2.0 Volt. Operation at such elevated current densities was found to have an impact on both cell design and water management. It is necessary to pressurize the cell to reduce the volumetric fractions of the gas flow and the porosity of the current collectors (Figure 1, 3-3') needs to be adjusted accordingly. Also, the water flow pumped through the cell must be adjusted to remove the excess heat produced inside the cell by internal

dissipation. In the future, the target point of 10 A.cm^{-2} at 2.0 volt will be reached by combining these different factors.

4. Conclusions and perspectives

Conventional PEM water electrolysis cells are currently operated over the 1-3 A.cm^{-2} range but technically, they can be operated close to (or above) 10 A.cm^{-2}. A cost analysis has been performed to show the interest of operating PEM cells up to 10 A.cm^{-2} current densities. It is necessary to adapt the cell design and to pump a sufficient amount of liquid water across the cell to extract the excess heat and to avoid gas screening effects: those requirements have been discussed in details. A correlation between the water flow and the maximum cell temperature has been derived. The role of operating pressure has been analyzed. I-V curves have been measured at current densities up to 10 A.cm^{-2}, using PFSA membranes of various thicknesses. These experimental I-V curves have been fitted with a model equation and key cell characteristics have been determined. It is shown that even when using thin (< 100 μm) PFSA materials, this leads to cell voltages close to 2.5-3.0 volt and to low cell efficiencies. Therefore R&D efforts are still needed to increase the cell efficiency at elevated current densities.

In terms of perspectives, innovative approaches are required to overcome existing limitations that stifle development in the field of PEM water electrolysis technology. From the electrochemical engineering viewpoint, there is a need to optimize the cell design and to reduce the internal resistance of non-MEA components to values less than 10-20 mΩ.cm^2. R&D efforts are also needed in material science to develop innovative electrocatalysts showing the appropriate activity and nano-architecture, and to get rid of noble metals, especially on the oxygen side, and to increase interface roughness. Efforts are also needed in polymer science to develop innovative proton-conducting membranes, with the appropriate proton conductivity, and showing a good compromise between thickness and gas

permeability. In particular, there is a need to develop thin (< 50 μm thick) and chemically stable (lifetimes of operation > 20,000 hours are needed) membranes that could operate up to 150°C and up to 50 bars with reduced gas cross-permeation flows to obtain sufficient efficiencies at elevated operating current densities. The contradictory trend between thickness and gas permeability reduces the chances to overcome the problem by tuning the properties of existing proton-conducting PFSA polymer materials. Another approach would be to improve existing nano-composite materials of reduced gas permeability.

Acknowledgement

Financial support from the French Agence Nationale de la Recherche (ANR 11 EMMA 048-01, ANR-RF-2015-01) and the French ADEME (Ademe 1694C006) is acknowledged.

Figure Captions

Figure 1. Schematic diagram showing the internal structure of a conventional PEM water electrolysis cell. (a) cathodic compartment; (b) membrane-electrode assembly (MEA); (c) anodic compartment.

Figure 2. (a) reference I-V curve and nominal set point; (b) hydrogen cost: (1) CAPEX; (b) OPEX; (3) total cost.

Figure 3. λ_{H2O} for (a) U^{cell} = 1.5 Volt; (b) U^{cell} = 1.6 Volt; (c) U^{cell} = 1.7; Volt; (d) U^{cell} = 1.8 Volt; (e) U^{cell} = 1.9 Volt

Figure 4. Volumetric fractions of liquid water (black curves) and gaseous oxygen (red curves) as a function of operating pressure, T = 65°C, and U^{cell} = 1.8 V for different cell ΔT: (a,a') 3°C ; (b,b') 10°C; (c,c') 20 °C.

Figure 5. I-V curves measured at 80°C and 1 atm on a 5-cells PEM water electrolysis short stack.

Figure 6. Volumetric fractions of liquid water and gaseous oxygen versus operating pressure (T=60°C, n=4).

Figure 7. (a) reference I-V curve with Nafion® 117 and (b) plot of the first order j derivative of curve (a). (1) specific resistance of the polymer electrolyte; (2) specific resistance of the cell. T = 80°C.

Figure 8. PEM water electrolysis I-V curves at 80°C and 15 bars. (●) experimental data points; (─) numerical fits; (----) limits of the different I-V domains of operation: (I) not accessible I-V domain; (II) conventional I-V domain of operation; (III) high I-V domain of operation; (IV) target I-V domain of operation.

References

[1] V. Petit, *The Energy Transition: an Overview of the True Challenges of the 21st Century*, Springer International Publishing, 2017.

[2] T. Bradford, *Solar revolution: The Economic Transformation of the Global Energy Industry*, MIT Press, 2006.

[3] M. Aklin, J. Urpelainen, *Renewables: the Politics of a Global Energy Transition*, MIT Press, 2018.

[4] M. Welsch, *Europe's Energy Transition: Insights for Policy Making*, Academic Press, 2017.

[5] O. Akizu, L. Urkidi, G. Bueno, R. Lago, *Tracing the emerging, energy transition in the Global North and the Global South*, Int. J. Hydrogen Energy, 42(28) (2017) 18046-18063.

[6] J. Michalski, U. Bünger, F. Crotogino, S. Donadei, G. S. Schneider, T. Pregger, K. K. Cao, D. Heide, , *Hydrogen generation by electrolysis and storage in salt caverns: Potentials, economics and sytems aspects with regard to the German energy transition*, Int. J. Hydrogen Energy, 42(19) (2017) 13427-13443.

[7] S. Weidner, M. Faltenbacher, I. François, D. Thomas, *Feasibility study of large scale hydrogen power-to-gas applications and cost of the systems evolving with scaling up in Germany, Belgium and Iceland*, Int. J. Hydrogen Energy, 43(33) (2018) 15625-15638.

[8] J. Rifkin, *The Hydrogen Economy: the Creation of the Worldwide Energy Web and the Redistribution of Power on Earth*, Polity Press (UK), 2003.

[9] S. Bennoua, A. Le Duigou, M. –M. Quéméré, S. Dautremont, *Role of hydrogen in resolving grid issues*, Int. J. Hydrogen Energy, 40(23) (2015) 7231-7245.

[10] P. Millet, Final report of the GenHyPEM research project, STREP n°019802, FP6, FCH-JU, European Commission, Brussel, Belgium (2008).

[11] P. Millet, final report of the HydroPEM project (ANR 11 EMMA 048 01), Agence Nationale de la Recherche, France (2011-2014).

[12] P. Millet, *In-situ electrochemical characterization of PEM Water Electrolysis electrodes*, Proceed. 1st Int. Workshop on Durability and Degradation Issues in PEM Electrolysis Cells and their Components, March 11-12, 2013, Freiburg, Germany.

[13] K. Lewinsky, PEM water Electrolysis for hydrogen production: Principles and Applications, chapter 5, *3M NSTF for PEM water electrolysis*, D. Bessarabov, H. Wand, H. Li, N. Zhao Ed., CRC Press, Boca Raton, USA (2016).

[14] L. Nereng *et al.*, *Operation of low-temp electrolyzers at very high current densities: A pipe dream or an opportunity?*, Proceed. 1st International Conference on Water Electrolysis, 2017 June 12–15; Copenhagen, Denmark.

[15] C. Rozain, P. Millet, *Electrochemical characterization of Polymer Electrolyte Membrane Water Electrolysis Cells*, Electrochimica Acta, 131 (2014) 160-167.

[16] *EU Harmonised Terminology for Low Temperature Water Electrolysis for Energy Storage Applications*, G. Tsotridis and A. Pilenga Edts., JRC science for policy report, European Commission, Luxembourg, In press.

[17] P. Millet, *Conventional and Innovative Electrocatalysts for PEM Water Electrolysis*, ECS Transaction, 75 (2016) 28-35.

[18] J. O'M. Bockris, A.K.N. Reddy, *Modern Electrochemistry*, Plenum Rosetta Ed., 1977.

[19] *Multi-Annual Work Program 2014-2020*, ID 4221004, Fuel Cells and Hydrogen Joint Undertaking, European Commission, 2013.

[20] S.M. Saba, M. Müller, M. Robinius, D. Stolten, *The investment cost of electrolysis- A comparison of cost studies over the past 30 years*, Int. J. Hydrogen Energy, 38 (2018) 1209-1223.

[21] P. Millet, A. Ranjbari, F. de Guglielmo, S.A. Grigoriev, F. Auprêtre, *Cell failure mechanisms in PEM water electrolyzers*, Int. J. Hydrogen Energy, 37 (2012) 17478-17487.

[22] W.H.Press, B.P. Flannery, SA Teukolsky, W.T. Vetterling, Numerical recipes, the art of scientific computing, Cambridge University Press, 1986.

[23] M. Schalenbach, M. Carmo, D.L. Fritz, J. Merel, D. Stolten, *Pressurized PEM water electrolysis: Efficiency and gas crossover*, Int. J. Hydrogen Energy, 38 (35) (2013) 14921-14933.

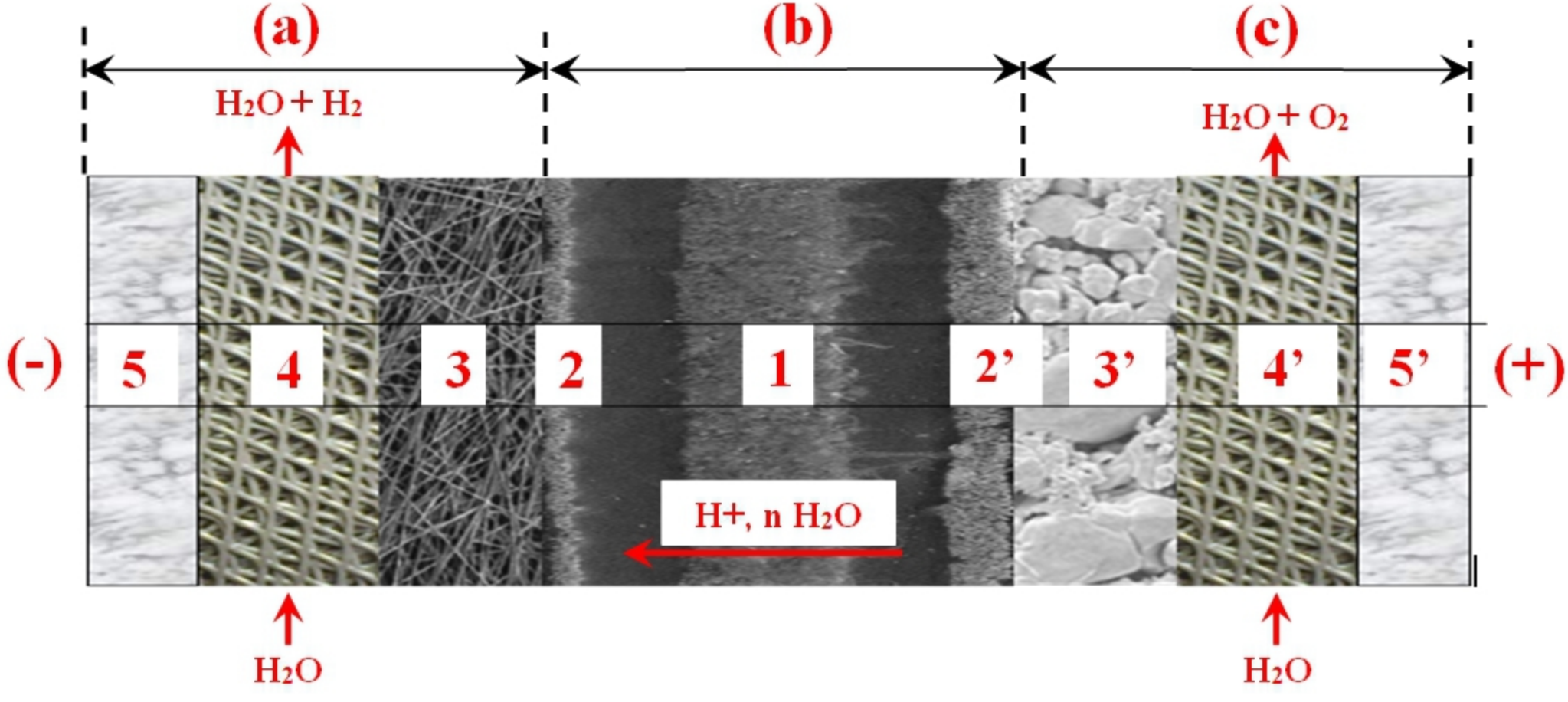
(a)
(b)
(c)
H₂O + H₂
H₂O + O₂
(-)
5
4
3
2
1
2'
3'
4'
5'
(+)
H+, n H₂O
H₂O
H₂O

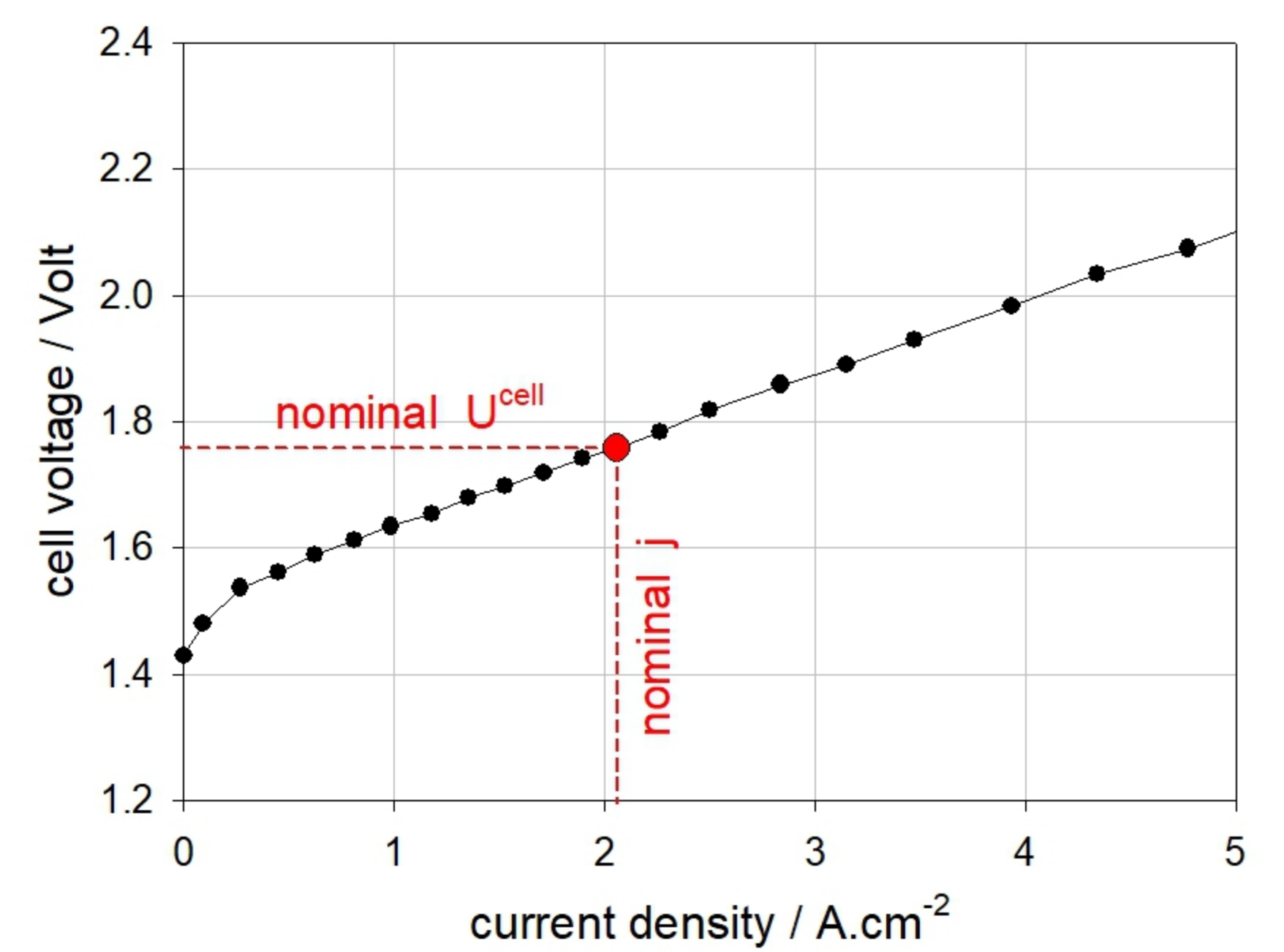
2.4
2.2
2.0
1.8
1.6
1.4
1.2
cell voltage / Volt
nominal U^cell
nominal j
0
1
2
3
4
5
current density / A.cm^-2

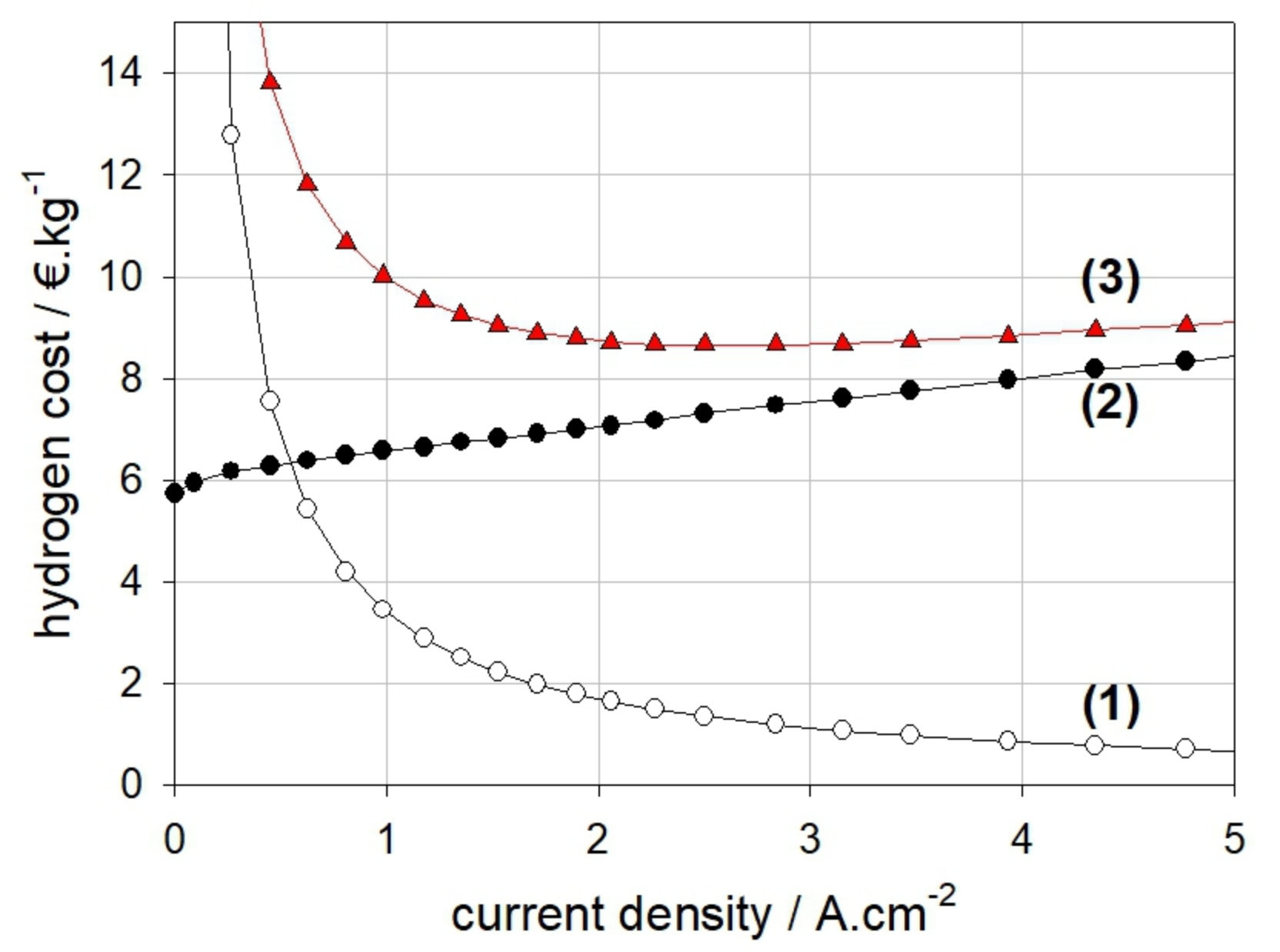
hydrogen cost / €.kg-1
14
12
10
8
6
4
2
0
0
1
2
3
4
5
current density / A.cm-2
(3)
(2)
(1)

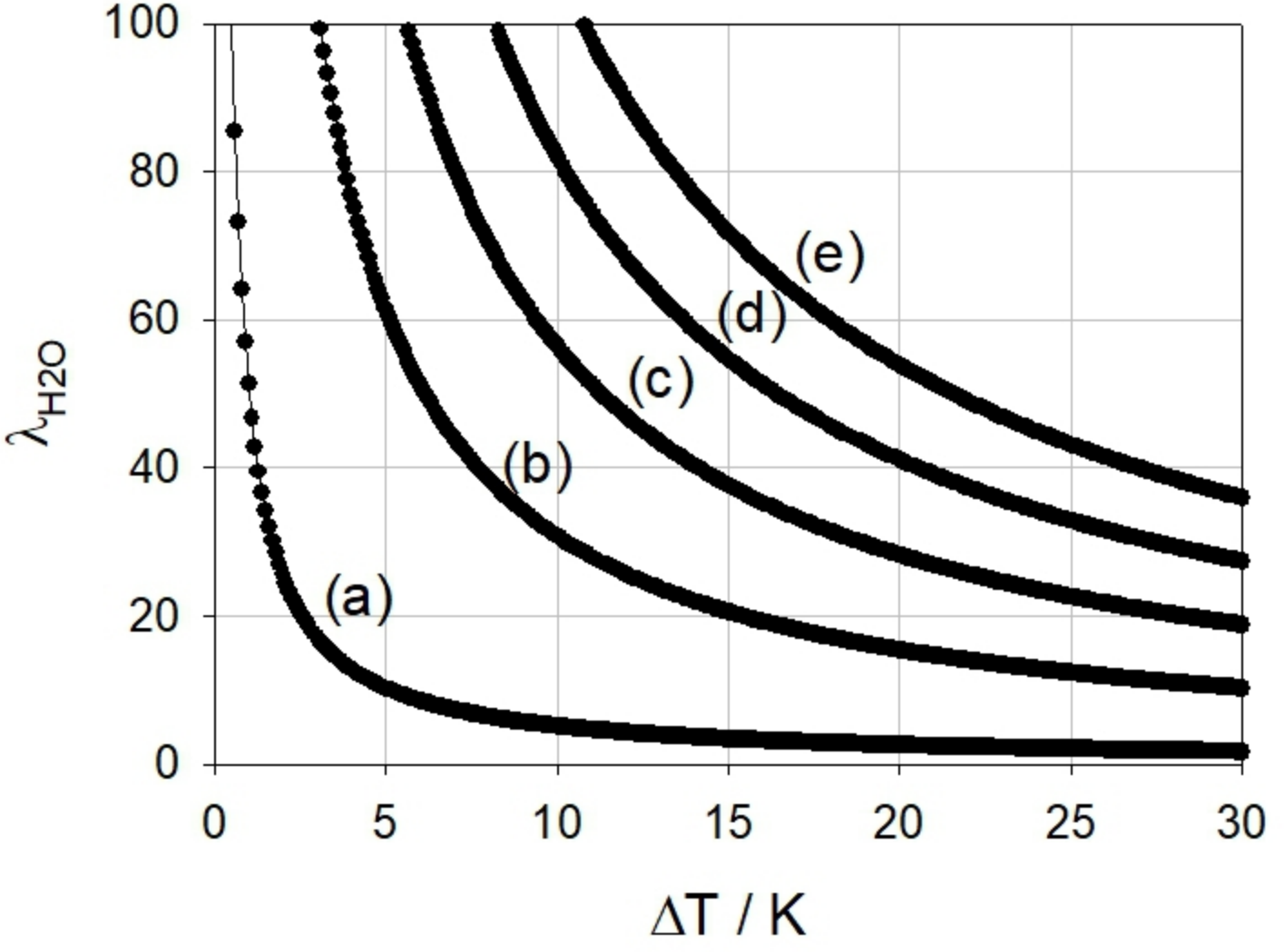
100
80
60
40
20
0
λ_{H2O}
0
5
10
15
20
25
30
ΔT / K
(a)
(b)
(c)
(d)
(e)

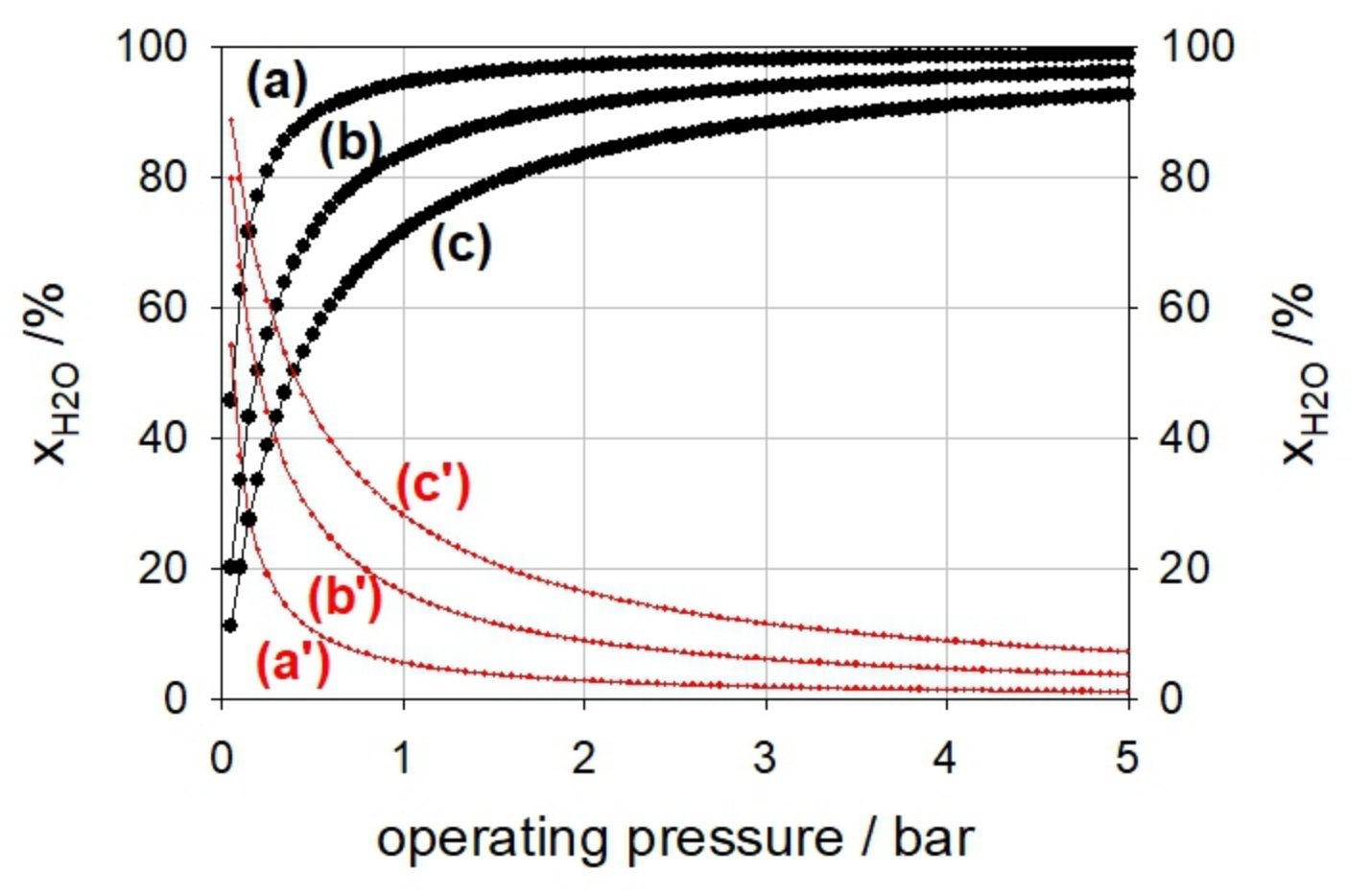
100
80
60
40
20
0
(a)
(b)
(c)
(c')
(b')
(a')
x_{H2O} /%
0
1
2
3
4
5
operating pressure / bar

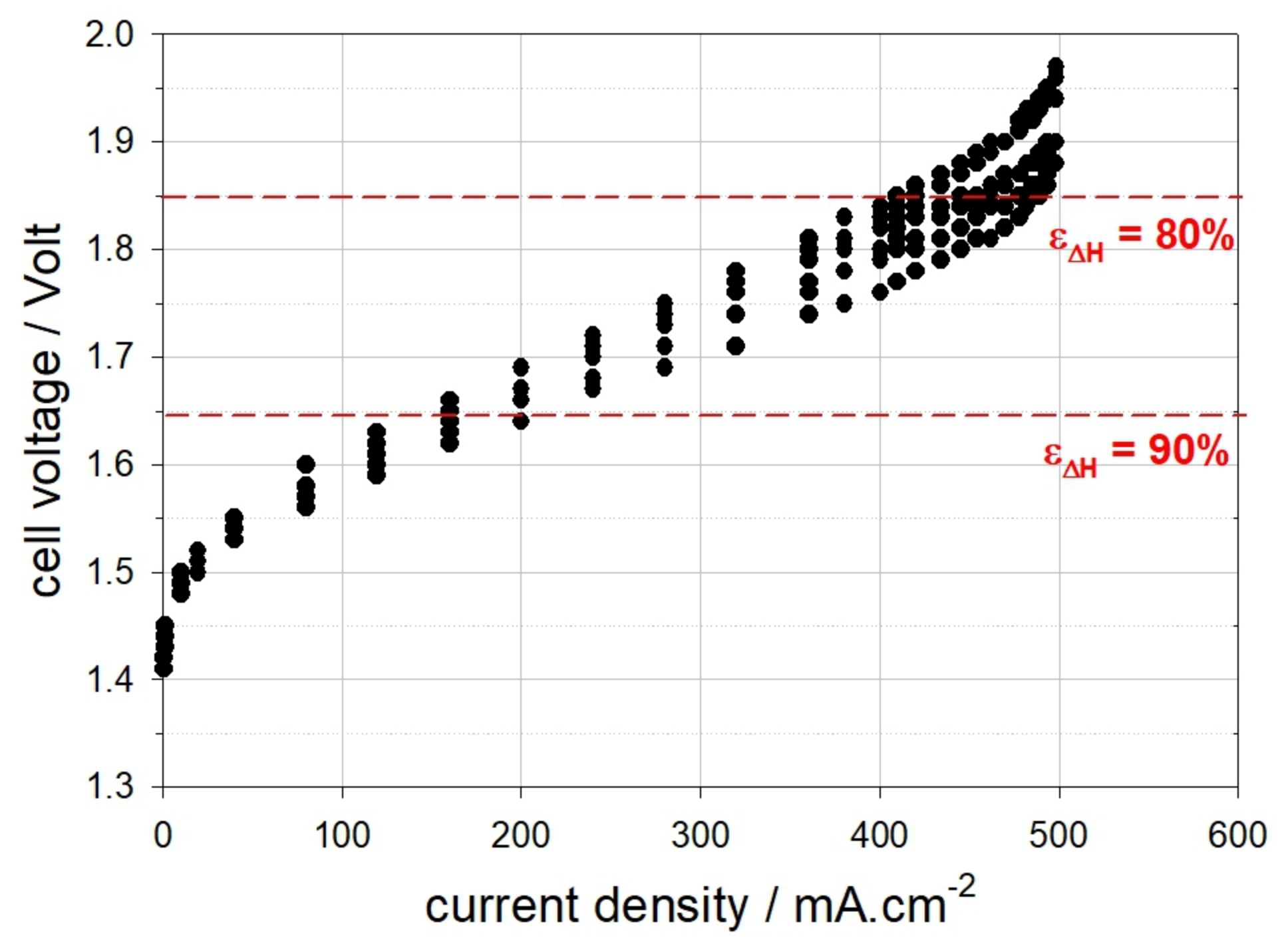
2.0
1.9
1.8
1.7
1.6
1.5
1.4
1.3
cell voltage / Volt
0
100
200
300
400
500
600
current density / mA.cm-2
εΔH = 80%
εΔH = 90%

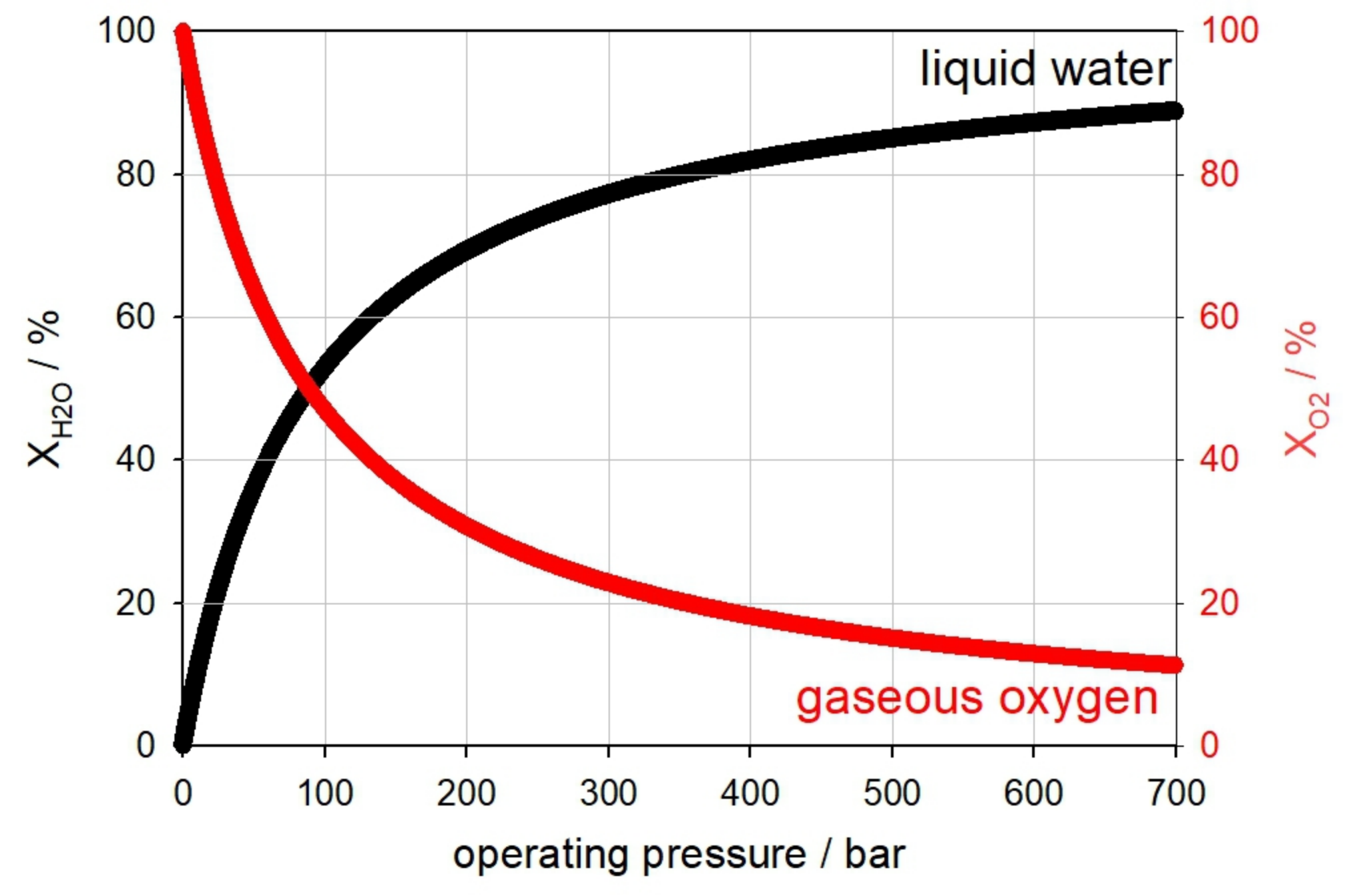
liquid water
gaseous oxygen
X_{H2O} / %
X_{O2} / %
operating pressure / bar
0
20
40
60
80
100
0
100
200
300
400
500
600
700

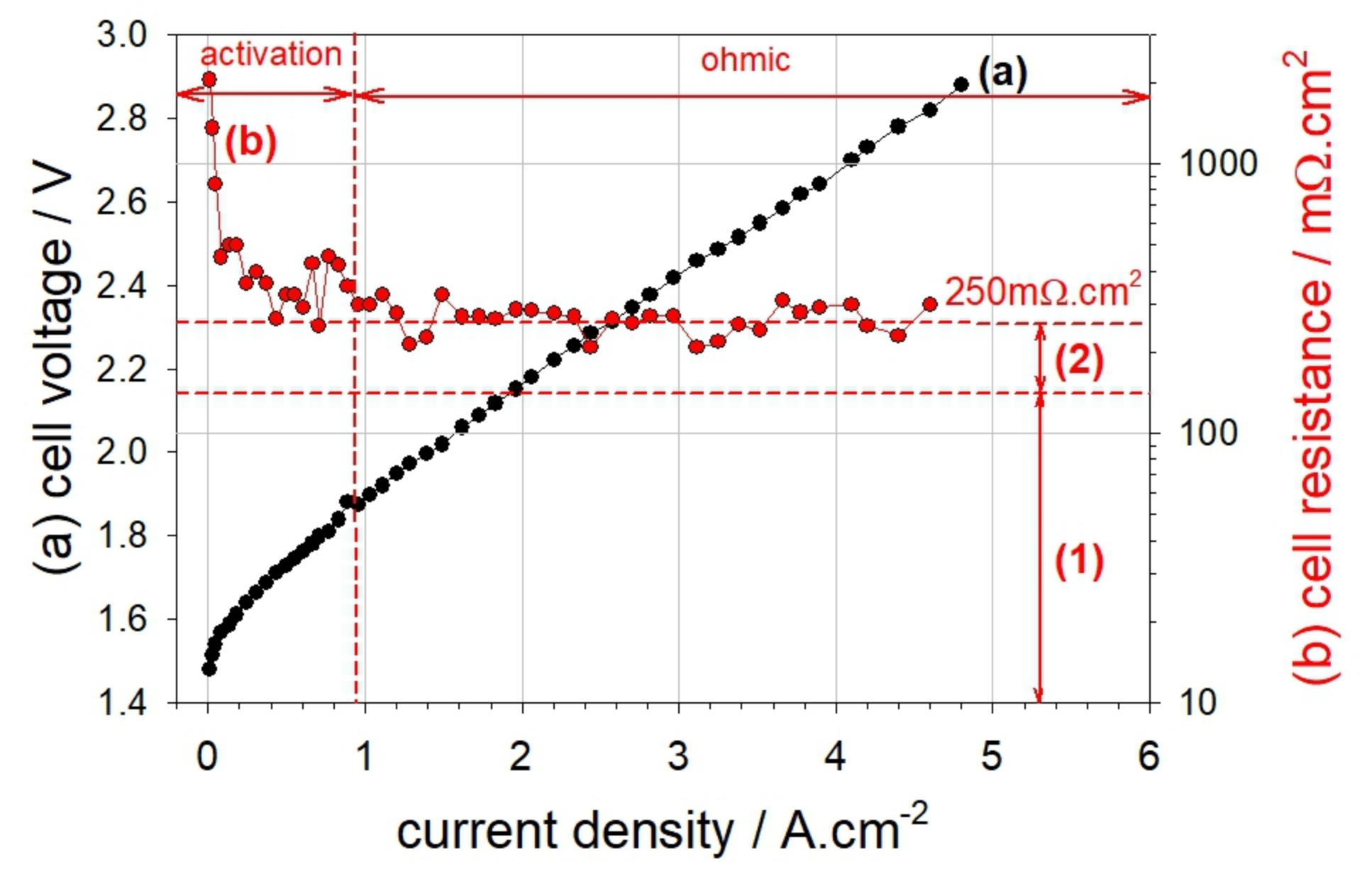
activation
ohmic
(a)
(b)
250mΩ.cm²
(2)
(1)
(a) cell voltage / V
(b) cell resistance / mΩ.cm²
current density / A.cm⁻²
3.0
2.8
2.6
2.4
2.2
2.0
1.8
1.6
1.4
1000
100
10
0
1
2
3
4
5
6

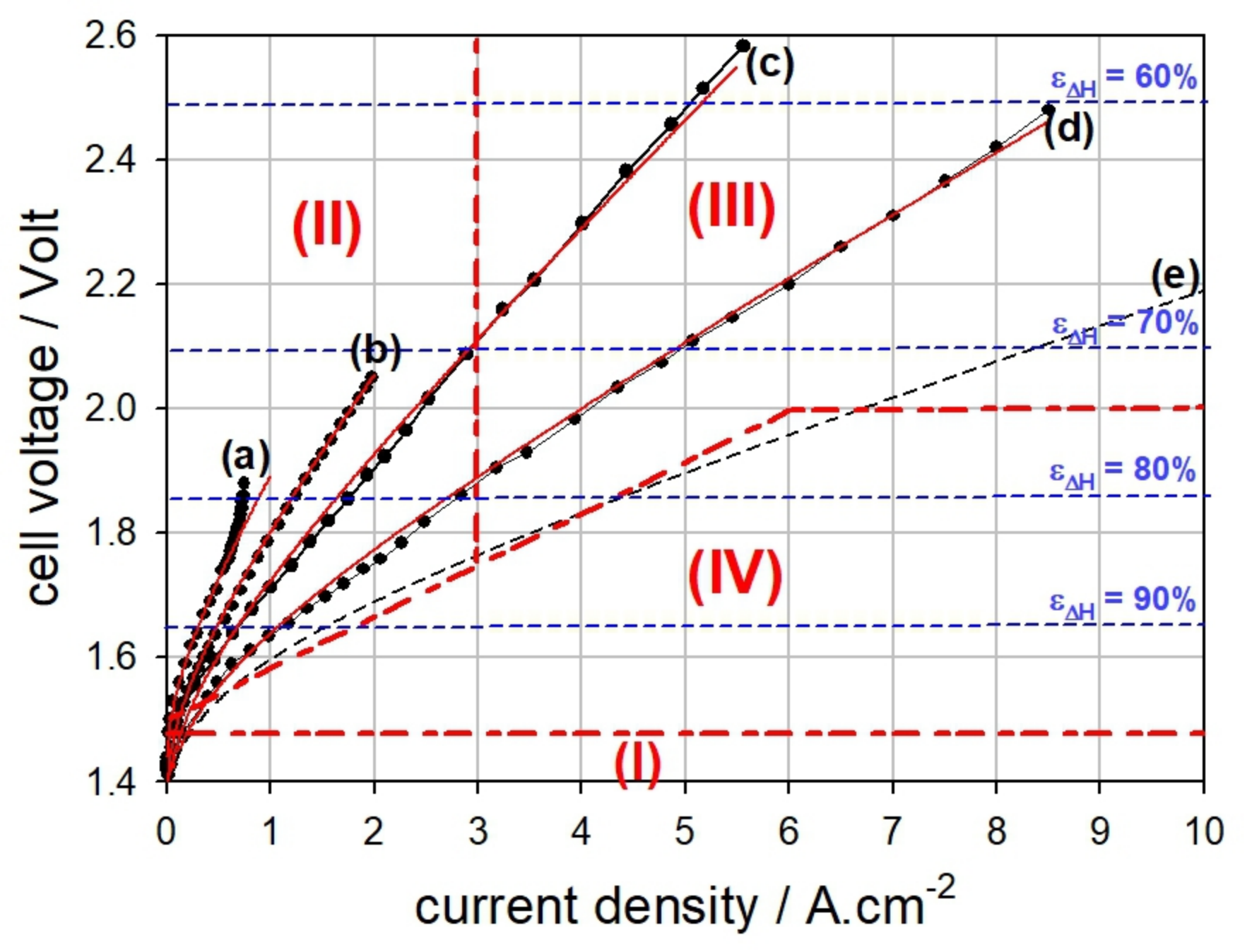
cell voltage / Volt
current density / A.cm-2
2.6
2.4
2.2
2.0
1.8
1.6
1.4
0
1
2
3
4
5
6
7
8
9
10
(a)
(b)
(c)
(d)
(e)
(I)
(II)
(III)
(IV)
εΔH = 60%
εΔH = 70%
εΔH = 80%
εΔH = 90%

Table 1. Fit parameters of the I-V curves of Figure 8.

	Membrane dry thickness (μm)	Temperature (°C)	R_{cell} ($m\Omega.cm^2$)	j_0^a ($A.cm^{-2}$)	r_f^a (adim)	i_0^c ($A.cm^{-2}$)	r_f^c (adim)
curve (a)	178	80	250	10^{-6}	5	10^{-3}	150
curve (b)	178	80	210	10^{-6}	25	10^{-3}	150
curve (c)	127	80	160	10^{-6}	60	10^{-3}	150
curve (d)	51	80	92	10^{-6}	75	10^{-3}	150
curve (e)	25	80	50	10^{-6}	75	10^{-3}	210